Mechanized azobenzene-functionalized zirconium metal-organic framework for on-command cargo release

Xiangshi Meng,[1]* Bo Gui,[1]* Daqiang Yuan,[2] Matthias Zeller,[3] Cheng Wang[1]†

Stimuli-responsive metal-organic frameworks (MOFs) have gained increasing attention recently for their potential applications in many areas. We report the design and synthesis of a water-stable zirconium MOF (Zr-MOF) that bears photoresponsive azobenzene groups. This particular MOF can be used as a reservoir for storage of cargo in water, and the cargo-loaded MOF can be further capped to construct a mechanized MOF through the binding of β-cyclodextrin with the azobenzene stalks on the MOF surface. The resulting mechanized MOF has shown on-command cargo release triggered by ultraviolet irradiation or addition of competitive agents without premature release. This study represents a simple approach to the construction of stimuli-responsive mechanized MOFs, and considering mechanized UiO-68-azo made from biocompatible components, this smart system may provide a unique MOF platform for on-command drug delivery in the future.

INTRODUCTION

Stimuli-responsive molecules, which are capable of changing their structures and/or properties in response to external stimuli such as light (1–3), pH (4, 5), chemicals (6), etc., have attracted intensive attention because of their important role for the construction of functional materials. Azobenzene, as one of the most studied photochromic molecules, can be switched from the thermally stable trans isomer to the metastable cis isomer under photoirradiation (7). During this process, the azobenzene unit undergoes significant changes in the structure and polarity of the molecule, which can result in azobenzene-containing materials with interesting photoresponsive behavior. A variety of systems [for example, polymers (8–10), liquid crystals (11, 12), nanoparticles (13), etc.] that bear azobenzene units have been developed, and these smart materials have shown promising applications in many areas, including optical data storage devices (14, 15) and on-command drug delivery (16–18).

Metal-organic frameworks (MOFs) (19–21), a new class of porous crystalline materials constructed from metal ions and organic ligands, have been widely used in gas storage and separation (22–25), in catalysis (26–28), as sensors (29–31), and in drug delivery (32–34). Stimuli-responsive MOFs, which can show response to external stimuli with a detectable change in physical and/or chemical properties, have gained increasing attention recently for their potential applications in many areas (35–43). An attractive way to construct these smart MOFs is by incorporating the stimuli-responsive molecules into the framework as organic linkers (44). Starting from ligands functionalized with azobenzene units as a dangling group, several azobenzene-containing photochromic MOFs with interesting tunable properties have been reported over the past few years (45–48). For example, Zhou et al. (46) reported an azobenzene-functionalized MOF with MOF-5 topology, which can absorb different amounts of CO_2 after ultraviolet (UV) or heat treatment. Yaghi et al. (47) reported another azobenzene-based MOF with an MOF-74 structure

that can release dyes from its pores after photoirradiation. However, the stability of these photoresponsive MOFs in different environments (for example, water) is still a major challenge that keeps these compounds from being used more widely. Considering their interesting properties and applications, more azobenzene-based MOFs with high stability are in great demand.

Herein, we report the design and synthesis of a water-stable zirconium MOF (Zr-MOF) that bears azobenzene groups, namely, UiO-68-azo (Fig. 1). This MOF can be used as a reservoir for cargo storage in water, and the cargo-loaded MOF can be further capped to construct a mechanized MOF through the binding of β-cyclodextrin (β-CD), with the azobenzene stalks protruding from the surface of UiO-68-azo. Because the bulky supramolecular complexes are located near the pore openings, the pores are sealed, thus stopping the spontaneous release of cargo trapped inside. The resulting mechanized MOF shows on-command cargo release upon external chemical or physical stimuli because of the dissociation of β-CD rings from the azobenzene stalks on the MOF surface. We believe that this proof-of-concept research does not only represent a simple approach to the construction of stimuli-responsive mechanized MOFs, but it may also provide a unique MOF platform for on-command drug delivery.

RESULTS AND DISCUSSION

To construct a stimuli-responsive MOF with large enough cavities for efficient azobenzene photoisomerization, we designed and synthesized a novel ligand that bears an azobenzene unit as dangling group, 2′-p-tolyldiazenyl-1,1′:4,4′-terphenyl-4,4″-dicarboxylic acid (1; Fig. 1 and see fig. S1 for synthesis). From the absorption spectroscopy (fig. S2) and ^{1}H nuclear magnetic resonance (NMR) spectroscopy (fig. S3), ligand 1 can undergo a trans-to-cis isomerization in solution when exposed to UV light. To ensure structural integrity of the framework during the stimulation process, we chose to construct the Zr-MOFs (49), which are known for their robustness, for example, water stability. Moreover, Zr-MOFs are biocompatible and degradable, having a wide array of potential applications in drug delivery (50). After treatment of a reaction mixture containing

[1]Key Laboratory of Biomedical Polymers of Ministry of Education, College of Chemistry and Molecular Sciences, Wuhan University, Wuhan 430072, China. [2]State Key Laboratory of Structural Chemistry, Fujian Institute of Research on the Structure of Matter, Chinese Academy of Sciences, Fuzhou 350002, China. [3]Department of Chemistry, Purdue University, 560 Oval Drive, West Lafayette, IN 47907, USA.
*These authors contributed equally to this work.
†Corresponding author. Email: chengwang@whu.edu.cn

ligand **1**, ZrCl₄, acetic acid, and dimethylformamide (DMF) at 100°C for 72 hours, UiO-68-azo was obtained as red octahedron-shaped crystals in reasonable yield. Single-crystal x-ray diffraction studies revealed a UiO-type structure for UiO-68-azo (Fig. 2A and table S1), which crystallizes in the $Fm\bar{3}m$ space group and contains a three-dimensional percolated pore structure. Because of the positional disorder and the flexible nature of the dangling substituents, the azobenzene groups

could not be located in the electron density map. Instead, their presence was established and quantified by ¹H NMR spectrum of digested MOF samples. As shown in fig. S4, the ¹H NMR spectroscopy of digested UiO-68-azo is the same as that of ligand **1** (fig. S5), indicating that the intactness of ligands in the MOF. In addition, powder x-ray diffraction (PXRD) patterns of UiO-68-azo (Fig. 3) are closely matched with that simulated from the single-crystal structure. Nitrogen sorption measurement of
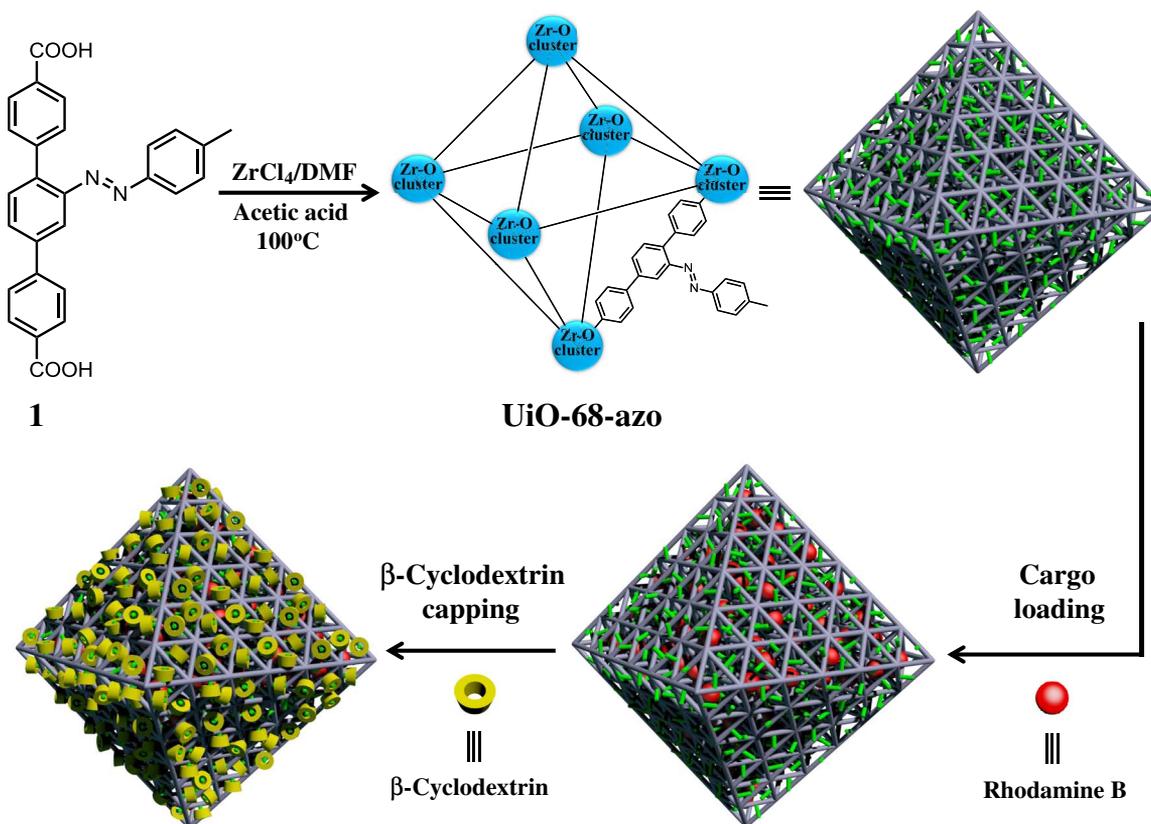

Fig. 1. Schematic representation. Schematic illustration of the synthesis of UiO-68-azo and further construction of RhB-loaded, β-CD–capped UiO-68-azo with azobenzene units as stalks encircled by β-CD on the surface. The trans-azobenzene is colored in green.
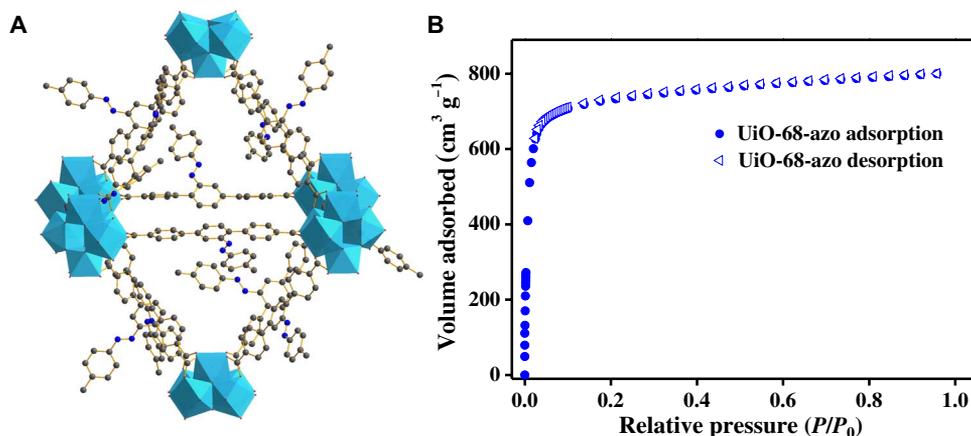

Fig. 2. Crystal structure and gas absorption behavior. (**A**) Crystal structure of UiO-68-azo. The azobenzene units were not located in the electron density map and are instead presented in an optimized position. (**B**) N₂ adsorption isotherms of activated UiO-68-azo.

UiO-68-azo at 77 K was performed to confirm its permanently porous nature (Fig. 2B and fig. S6). The Brunauer-Emmett-Teller (BET) analysis gave a high surface area of 2900 $m^2 g^{-1}$ and a pore volume of 1.24 $cm^3 g^{-1}$, demonstrating the potential application of UiO-68-azo in cargo storage. On the basis of the nonlocal density functional theory model, the pore size distribution of UiO-68-azo exhibits a relatively broad peak centered at 1.4 nm (fig. S7).

β-CD, which is composed of seven D-glucopyranosyl units and biocompatible (51), is well known to form complexes in the aqueous solution with a wide range of guest molecules (52). For example, it can form a supramolecular complex with azobenzene in water (2). Upon mixing of β-CD with cargo-loaded UiO-68-azo in water, the β-CD rings can thread onto the azobenzene stalks on the surface, thus serving as a gatekeeper to seal the nanopores and stop the release of the cargo. Furthermore, this inclusion complex can, in turn, again be disassembled when faced with the right external stimuli, which will open the nanovalves and then release the cargo inside (2). Therefore, we decided to construct a stimuli-responsive mechanized MOF based on UiO-68-azo. We chose rhodamine B (RhB) as the cargo because it matches the pore aperture of UiO-68-azo (fig. S7) and can also diffuse into the framework through its triangle windows (fig. S8). After immersing UiO-68-azo in an RhB aqueous solution and then rinsing with β-CD aqueous solution (Fig. 1), an RhB-loaded, β-CD–capped UiO-68-azo was obtained. As shown in Fig. 3, the position of the PXRD peaks of this mechanized MOF is similar to that of UiO-68-azo, pointing toward retention of the framework architecture.

We then investigated the on-command release behavior of RhB-loaded, β-CD–capped UiO-68-azo in water. Because β-CD shows a much higher binding affinity toward trans-azobenzene compared with cis-azobenzene in water (16), the isomerization of azobenzene from trans-to-cis can forc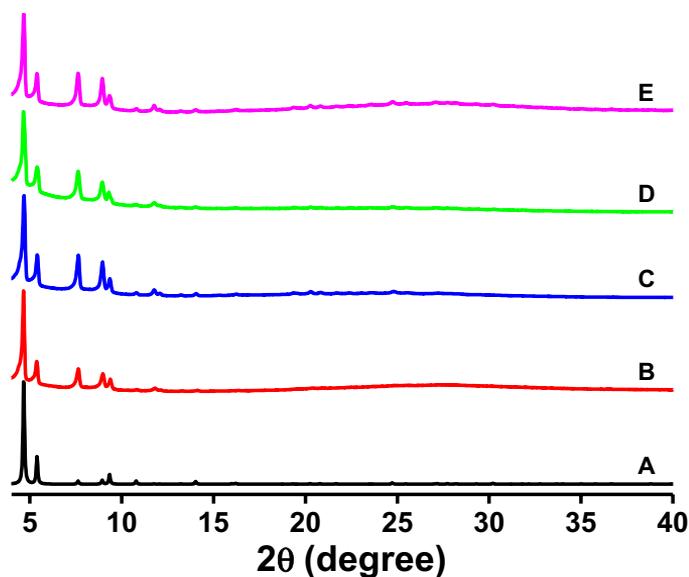e β-CD rings away from the stalks, thus opening the gates to the nanopores and releasing the cargo (Fig. 4A). Therefore, we studied the light-trigged release profile of this mechanized MOF, which was monitored by measuring the absorption intensity of the released RhB as a function of time (Fig. 4B and fig. S9). Before UV irradiation, a flat baseline was found, showing that the RhB molecules are held firmly within the nanopores of the mechanized MOF without premature release. When the UV light was turned on, the release of the RhB cargo was observed, demonstrating that the supramolecular nanovalves on the MOF surface are opened. The release process began to level off after 120 min, and PXRD (Fig. 3) again confirmed the retention of the framework during this process. It can be concluded that the controlled release of RhB cargos can be triggered by UV irradiation because of the dissociation of β-CD rings from the stalks on the MOF surface. We should mention here that, for the uncapped RhB-loaded UiO-68-azo, the RhB cargo can be spontaneously released from the nanopores of UiO-68-azo (fig. S10), indicating again the importance of the supramolecular β-CD azobenzene complex on the MOF surface.

The dissociation of β-CD rings from the azobenzene stalks of UiO-68-azo can also be triggered by the addition of a competitive binding agent (Fig. 5A), for example, amantadine, a drug that is used to treat Parkinson's disease and that has a higher binding affinity toward β-CD compared with azobenzene toward β-CD (52). As shown in Fig. 5B and fig. S11, the release of RhB was observed after the addition of amantadine and began to level off after 110 min as a result of the amantadine-induced dethreading of the β-CD rings from the azobenzene stalks. We should emphasize here that, if we chose agents (52) that have a much lower
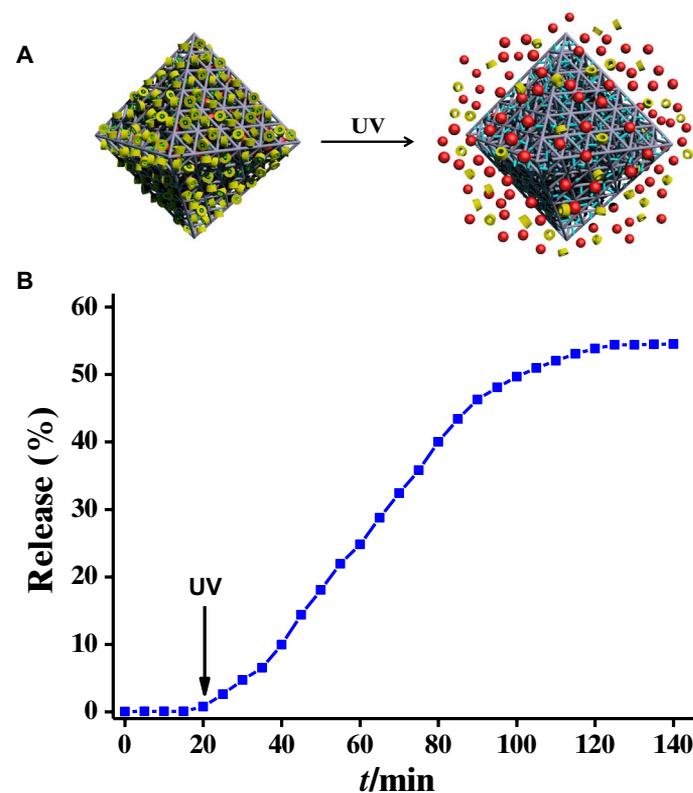
Fig. 3. PXRD patterns. (**A** to **E**) Simulated from the crystal structure of UiO-68-azo (A), fresh UiO-68-azo (B), RhB-loaded, β-CD–capped UiO-68-azo (C), RhB-loaded, β-CD–capped UiO-68-azo after UV irradiation (D), and RhB-loaded, β-CD–capped UiO-68-azo after addition of amantadine and then UV irradiation (E). The patterns were taken with crystals covered by a thin layer of water.

Fig. 4. On-command release. (**A**) Schematic illustration of the light-triggered release. The cis-azobenzene is colored in cyan. (**B**) Release profiles of RhB-loaded, β-CD–capped UiO-68-azo by UV irradiation.
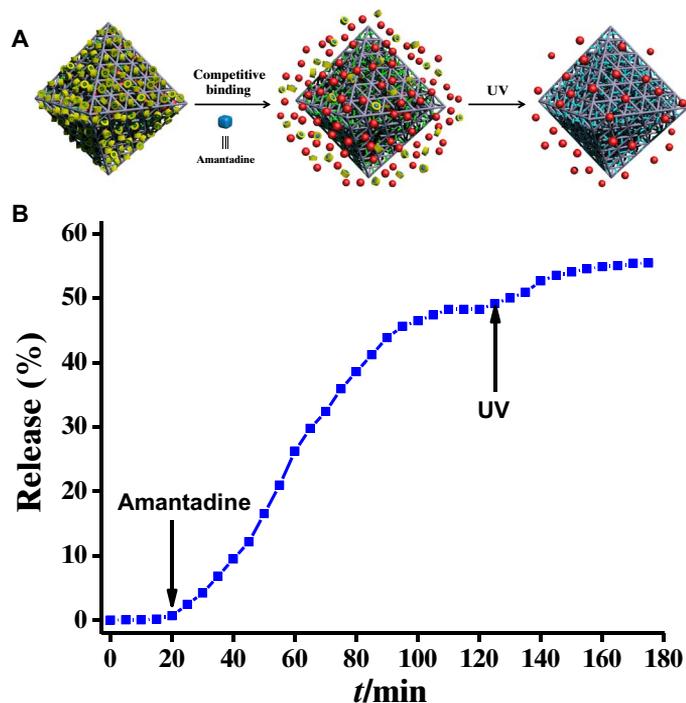
Fig. 5. Step-by-step on-command release. (**A**) Schematic illustration of the step-by-step release. The cis-azobenzene is colored in cyan. (**B**) Release profiles of RhB-loaded, β-CD–capped UiO-68-azo by addition of amantadine and then UV irradiation.

binding constant with β-CD, only a negligible amount of RhB was released (figs. S12 to S17), indicating again that the amantadine-triggered release is caused by the dissociation of β-CD rings from azobenzene stalks on the MOF surface. Because the isomerization of azobenzene from trans-to-cis can change the pore environment (46, 47) and may impel the guests out, the resultant system was further exposed to UV light (Fig. 5A). A re-emission of RhB cargo was observed (Fig. 5B), albeit only a small amount was detected. Therefore, the addition of amantadine can trigger the on-command release of RhB cargos, and additional UV irradiation impels additional RhB cargo out of the nanopores as a result of trans-to-cis isomerization.

CONCLUSION

In summary, we have reported the design and synthesis of a highly stable azobenzene-functionalized Zr-MOF, UiO-68-azo. The azobenzene units on the MOF surface can bind with β-CD to form a supramolecular complex, enabling UiO-68-azo to be used to construct a stimuli-responsive mechanized MOF without any premature release, simply by rinsing the cargo-loaded UiO-68-azo with β-CD aqueous solution. This supramolecular complex can be dissociated after subjecting it to different types of external stimuli, thus releasing the cargo inside the mechanized MOF in a controlled manner. We believe that this study represents a simple approach to the construction of stimuli-responsive mechanized MOFs. In addition, because the mechanized UiO-68-azo is constructed from biocompatible components (50, 51), this system may provide a unique MOF platform for on-command drug delivery. We are now

working on scaling down UiO-68-azo to nanoregime and studying the application of this mechanized MOF in on-command drug delivery.

MATERIALS AND METHODS

Materials

All reagents and solvents were purchased from commercial sources and used without further purification. Zirconium (IV) chloride (99.5%) was purchased from Alfa Aesar. 4-Methoxycarbonyl-phenylboronic acid, palladium acetate, 2,5-dibromoaniline, Na_2CO_3, NaOH, β-CD, RhB, D-arabinose, sodium benzoate, 4-amino-1-naphthalenesulfonic acid sodium salt, and Hepes were purchased from Admas. Dimethyl 2′-amino-1,1′:4,1″-terphenyl-4,4″-dicarboxylate (53) and p-nitrosotoluene (54) were synthesized according to the literature procedure.

Characterizations. ^1H and ^{13}C NMR spectra were measured on a Bruker Fourier 300 M and 400 M spectrometer. High-resolution mass spectra were collected on Bruker Daltonics Inc. APEXII FT-ICR mass spectrometer, which was equipped with EI (electron impact), ESI (electrospray ionization), and MALDI (matrix-assisted laser desorption ionization) as ionization source. PXRD data were collected on Rigaku SmartLab with Cu $K\alpha_1$ (λ = 1.54056 Å) radiation operated at 45 kV and 200 mA, from 2θ = 2° up to 50° with 0.02° increment. Single-crystal x-ray data were collected at 100 K at the Beijing Synchrotron Radiation Facility, beamline station 3W1A equipped with a MarCCD-165 detector. The UV irradiation experiment was performed by using the WHF 203 UV lamp (λ = 365 nm), which was put in a quartz vessel and cooled by continuous flowing water. The nitrogen adsorption and desorption isotherms of UiO-68-azo before and after UV irradiation were measured at 77 K using a Autosorb-iQ2 (Quantachrome) surface area and pore size analyzer. The specific surface areas were calculated from the adsorption data by using BET methods. The UV-visible absorption spectra were recorded on a Shimadzu UV-3600 spectrophotometer. Thermogravimetric analysis from 50° to 800°C was carried out on a DTA-60 Simultaneous DTG-TG Apparatus (Shimadzu) in air atmosphere using a 5°C/min ramp without equilibration delay.

Synthesis of UiO-68-azo. $ZrCl_4$ (23.1 mg, 0.099 mmol), ligand **1** (43.2 mg, 0.099 mmol), and acetic acid (1.1 ml) were dissolved in DMF (6 ml) in a 20-ml Pyrex vial. The mixture was placed in a preheated oven set at 100°C for 72 hours. Single crystals with octahedral shape suitable for single-crystal diffraction were harvested with a yield of ~20 mg. The crystals were washed with DMF over a 2-day period to remove any unreacted starting materials. After that, the samples were exchanged with H_2O for several times and then kept in H_2O before cargo loading. In addition, samples that were not used for cargo loading were immersed in anhydrous dichloromethane for 3 days to replace and remove DMF. These crystals were evacuated in oil pump vacuum at room temperature to yield activated samples.

Synthesis of RhB-loaded, β-CD–capped UiO-68-azo. A fresh sample of UiO-68-azo (~20 mg) was immersed in 15 ml of water solution containing RhB (15 mg ml^{-1}) for 12 hours in the dark. After decanting the solution, the sample was washed with some water and saturated β-CD solution (25 ml × 3) and then immersed in saturated β-CD solution for 3 hours. The RhB-loaded, β-CD–capped UiO-68-azo was isolated from solution through centrifugation, which was subsequently washed with water and then kept in water for on-command release study.

On-command release experiments. In a typical experiment, RhB-loaded, β-CD–capped UiO-68-azo was put in a vial and filled with deionized water, which was further subjected to UV irradiation or

addition of amantadine and then UV irradiation. To monitor the release of RhBs, the UV-visible spectra of the solutions were recorded every 5 min.

SUPPLEMENTARY MATERIALS

fig. S1. Synthesis of ligand **1**.
fig. S2. UV-visible spectra of ligand **1** after exposure to UV light for different times.
fig. S3. ^1H NMR spectra of ligand **1** before and after UV irradiation for 5 min.
fig. S4. ^1H NMR spectrum of digested UiO-68-azo.
fig. S5. ^1H NMR spectrum of ligand **1**.
fig. S6. N_2 sorption isotherm of UiO-68-azo at 77 K before and after UV irradiation for 3 hours.
fig. S7. Pore size distribution of UiO-68-azo before and after UV irradiation for 3 hours.
fig. S8. Size comparison of RhB and the pore windows of UiO-68-azo.
fig. S9. UV-visible spectra of the solution of mechanized UiO-68-azo after UV irradiation for different time.
fig. S10. Release profile of uncapped RhB-loaded UiO-68-azo.
fig. S11. UV-visible spectra of the solution of mechanized UiO-68-azo after addition of amantadine and then UV irradiation for different time.
fig. S12. Release study of mechanized UiO-68-azo after addition of D-arabinose.
fig. S13. Release study of mechanized UiO-68-azo after addition of 4-amino-1-naphthalenesulfonic acid sodium salt.
fig. S14. Release study of mechanized UiO-68-azo after addition of sodium benzoate.
fig. S15. Release study of mechanized UiO-68-azo after addition of ethanol.
fig. S16. Release study of mechanized UiO-68-azo after addition of acetone.
fig. S17. Release study of mechanized UiO-68-azo after addition of dimethyl sulfoxide.
fig. S18. Release profile of uncapped RhB-loaded UiO-68-azo after UV irradiation.
fig. S19. Release profile of uncapped RhB-loaded UiO-68-azo after addition of amantadine.
fig. S20. Release profile of uncapped RhB-loaded UiO-68-azo after addition of D-arabinose.
fig. S21. Thermogravimetric plot of UiO-68-azo.
fig. S22. UV-visible spectra of Hepes buffer solution containing UiO-68-azo with different time.
fig. S23. PXRD pattern of UiO-68-azo after being kept in a Hepes buffer solution for 3 hours.
table S1. Crystal data and structure refinement for UiO-68-azo.
Experiment details
Simulation details

REFERENCES AND NOTES

1. M. Irie, T. Fukaminato, K. Matsuda, S. Kobatake, Photochromism of diarylethene molecules and crystals: Memories, switches, and actuators. *Chem. Rev.* **114**, 12174–12277 (2014).
2. D.-H. Qu, Q.-C. Wang, Q.-W. Zhang, X. Ma, H. Tian, Photoresponsive host–guest functional systems. *Chem. Rev.* **115**, 7543–7588 (2015).
3. M. Baroncini, S. d'Agostino, G. Bergamini, P. Ceroni, A. Comotti, P. Sozzani, I. Bassanetti, F. Grepioni, T. M. Hernandez, S. Silvi, Photoinduced reversible switching of porosity in molecular crystals based on star-shaped azobenzene tetramers. *Nat. Chem.* **7**, 634–640 (2015).
4. S. Grunder, P. L. McGrier, A. C. Whalley, M. M. Boyle, C. Stern, J. F. Stoddart, A water-soluble pH-triggered molecular switch. *J. Am. Chem. Soc.* **135**, 17691–17694 (2013).
5. X. Yan, P. Wei, Z. Li, B. Zheng, S. Dong, F. Huang, Q. Zhou, A dynamic [1]catenane with pH-responsiveness formed via threading-followed-by-complexation. *Chem. Commun.* **49**, 2512–2514 (2013).
6. H. Maeda, Y. Bando, K. Shimomura, I. Yamada, M. Naito, K. Nobusawa, H. Tsumatori, T. Kawai, Chemical-stimuli-controllable circularly polarized luminescence from anion-responsive π-conjugated molecules. *J. Am. Chem. Soc.* **133**, 9266–9269 (2011).
7. H. M. D. Bandara, S. C. Burdette, Photoisomerization in different classes of azobenzene. *Chem. Soc. Rev.* **41**, 1809–1825 (2012).
8. H. Chen, X. Ma, S. Wu, H. Tian, A rapidly self-healing supramolecular polymer hydrogel with photostimulated room-temperature phosphorescence responsiveness. *Angew. Chem. Int. Ed.* **53**, 14149–14152 (2014).
9. S. Iamsaard, S. J. Aßhoff, B. Matt, T. Kudernac, J. J. L. M. Cornelissen, S. P. Fletcher, N. Katsonis, Conversion of light into macroscopic helical motion. *Nat. Chem.* **6**, 229–235 (2014).
10. L. Yang, Y. Bai, X. Tan, Z. Wang, X. Zhang, Controllable supramolecular polymerization through host–guest interaction and photochemistry. *ACS Macro Lett.* **4**, 611–615 (2015).
11. Y. Wang, Q. Li, Light-driven chiral molecular switches or motors in liquid crystals. *Adv. Mater.* **24**, 1926–1945 (2012).
12. B. Soberats, E. Uchida, M. Yoshio, J. Kagimoto, H. Ohno, T. Kato, Macroscopic photocontrol of ion-transporting pathways of a nanostructured imidazolium-based photoresponsive liquid crystal. *J. Am. Chem. Soc.* **136**, 9552–9555 (2014).
13. H. Zhao, S. Sen, T. Udayabhaskararao, M. Sawczyk, K. Kučanda, D. Manna, P. K. Kundu, J.-W. Lee, P. Král, R. Klajn, Reversible trapping and reaction acceleration within dynamically self-assembling nanoflasks. *Nat. Nanotechnol.* **11**, 82–88 (2016).
14. S. Kawata, Y. Kawata, Three-dimensional optical data storage using photochromic materials. *Chem. Rev.* **100**, 1777–1788 (2000).
15. C. Raimondo, N. Crivillers, F. Reinders, F. Sander, M. Mayor, P. Samorì, Optically switchable organic field-effect transistors based on photoresponsive gold nanoparticles blended with poly(3-hexylthiophene). *Proc. Natl. Acad. Sci. U.S.A.* **109**, 12375–12380 (2012).
16. D. P. Ferris, Y.-L. Zhao, N. M. Khashab, H. A. Khatib, J. F. Stoddart, J. I. Zink, Light-operated mechanized nanoparticles. *J. Am. Chem. Soc.* **131**, 1686–1688 (2009).
17. J. Liu, W. Bu, L. Pan, J. Shi, NIR-triggered anticancer drug delivery by upconverting nanoparticles with integrated azobenzene-modified mesoporous silica. *Angew. Chem. Int. Ed.* **52**, 4375–4379 (2013).
18. X. Chi, X. Ji, D. Xia, F. Huang, A dual-responsive supra-amphiphilic polypseudorotaxane constructed from a water-soluble pillar[7]arene and an azobenzene-containing random copolymer. *J. Am. Chem. Soc.* **137**, 1440–1443 (2015).
19. S. Kitagawa, R. Kitaura, S.-i. Noro, Functional porous coordination polymers. *Angew. Chem. Int. Ed.* **43**, 2334–2375 (2004).
20. G. Férey, Hybrid porous solids: Past, present, future. *Chem. Soc. Rev.* **37**, 191–214 (2008).
21. H. Furukawa, K. E. Cordova, M. O'Keeffe, O. M. Yaghi, The chemistry and applications of metal-organic frameworks. *Science* **341**, 1230444 (2013).
22. N. L. Rosi, J. Eckert, M. Eddaoudi, D. T. Vodak, J. Kim, M. O'Keeffe, O. M. Yaghi, Hydrogen storage in microporous metal-organic frameworks. *Science* **300**, 1127–1129 (2003).
23. J.-R. Li, J. Sculley, H.-C. Zhou, Metal–organic frameworks for separations. *Chem. Rev.* **112**, 869–932 (2012).
24. J. Pang, F. Jiang, M. Wu, C. Liu, K. Su, W. Lu, D. Yuan, M. Hong, A porous metal-organic framework with ultrahigh acetylene uptake capacity under ambient conditions. *Nat. Commun.* **6**, 7575 (2015).
25. K. J. Hartlieb, J. M. Holcroft, P. Z. Moghadam, N. A. Vermeulen, M. M. Algaradah, M. S. Nassar, Y. Y. Botros, R. Q. Snurr, J. F. Stoddart, CD-MOF: A versatile separation medium. *J. Am. Chem. Soc.* **138**, 2292–2301 (2016).
26. M. Yoon, R. Srirambalaji, K. Kim, Homochiral metal–organic frameworks for asymmetric heterogeneous catalysis. *Chem. Rev.* **112**, 1196–1231 (2012).
27. T. Zhang, W. Lin, Metal–organic frameworks for artificial photosynthesis and photocatalysis. *Chem. Soc. Rev.* **43**, 5982–5993 (2014).
28. H. Fei, S. M. Cohen, Metalation of a thiocatechol-functionalized Zr(IV)-based metal–organic framework for selective C–H functionalization. *J. Am. Chem. Soc.* **137**, 2191–2194 (2015).
29. Z. Hu, B. J. Deibert, J. Li, Luminescent metal–organic frameworks for chemical sensing and explosive detection. *Chem. Soc. Rev.* **43**, 5815–5840 (2014).
30. F.-Y. Yi, J.-P. Li, D. Wu, Z.-M. Sun, A series of multifunctional metal–organic frameworks showing excellent luminescent sensing, sensitization, and adsorbent abilities. *Chemistry* **21**, 11475–11482 (2015).
31. Z. Hu, W. P. Lustig, J. Zhang, C. Zheng, H. Wang, S. J. Teat, Q. Gong, N. D. Rudd, J. Li, Effective detection of mycotoxins by a highly luminescent metal–organic framework. *J. Am. Chem. Soc.* **137**, 16209–16215 (2015).
32. J. Della Rocca, D. Liu, W. Lin, Nanoscale metal–organic frameworks for biomedical imaging and drug delivery. *Acc. Chem. Res.* **44**, 957–968 (2011).
33. P. Horcajada, R. Gref, T. Baati, P. K. Allan, G. Maurin, P. Couvreur, G. Férey, R. E. Morris, C. Serre, Metal–organic frameworks in biomedicine. *Chem. Rev.* **112**, 1232–1268 (2012).
34. L.-L. Tan, H. Li, Y. C. Qiu, D.-X. Chen, X. Wang, R.-Y. Pan, Y. Wang, S. X.-A. Zhang, B. Wang, Y.-W. Yang, Stimuli-responsive metal–organic frameworks gated by pillar[5]arene supramolecular switches. *Chem. Sci.* **6**, 1640–1644 (2015).
35. Y. Sakata, S. Furukawa, M. Kondo, K. Hirai, N. Horike, Y. Takashima, H. Uehara, N. Louvain, M. Meilikhov, T. Tsuruoka, Shape-memory nanopores induced in coordination frameworks by crystal downsizing. *Science* **339**, 193–196 (2013).
36. X.-L. Qi, S.-Y. Liu, R.-B. Lin, P.-Q. Liao, J.-W. Ye, Z. Lai, Y. Guan, X.-N. Cheng, J.-P. Zhang, X.-M. Chen, Phosphorescence doping in a flexible ultramicroporous framework for high and tunable oxygen sensing efficiency. *Chem. Commun.* **49**, 6864–6866 (2013).
37. S. S. Nagarkar, A. V. Desai, S. K. Ghosh, Stimulus-responsive metal–organic frameworks. *Chem. Asian J.* **9**, 2358–2376 (2014).
38. J. Gao, J. Miao, P.-Z. Li, W. Y. Teng, L. Yang, Y. Zhao, B. Liu, Q. Zhang, A p-type Ti(iv)-based metal–organic framework with visible-light photo-response. *Chem. Commun.* **50**, 3786–3788 (2014).
39. L.-L. Tan, H. Li, Y. Zhou, Y. Zhang, X. Feng, B. Wang, Y.-W. Yang, Zn²⁺-triggered drug release from biocompatible zirconium MOFs equipped with supramolecular gates. *Small* **11**, 3807–3813 (2015).
40. X.-G. Wang, Z.-Y. Dong, H. Cheng, S.-S. Wan, W.-H. Chen, M.-Z. Zou, J.-W. Huo, H.-X. Deng, X.-Z. Zhang, A multifunctional metal–organic framework based tumor targeting drug delivery system for cancer therapy. *Nanoscale* **7**, 16061–16070 (2015).

41. J. Yu, Y. Cui, C.-D. Wu, Y. Yang, B. Chen, G. Qian, Two-photon responsive metal–organic framework. *J. Am. Chem. Soc.* **137**, 4026–4029 (2015).

42. Q. Chen, Z. Chang, W.-C. Song, H. Song, H.-B. Song, T.-L. Hu, X.-H. Bu, A controllable gate effect in cobalt(II) organic frameworks by reversible structure transformations. *Angew. Chem. Int. Ed.* **52**, 11550–11553 (2013).

43. H. Wang, J. Xu, D.-S. Zhang, Q. Chen, R.-M. Wen, Z. Chang, X.-H. Bu, Crystalline capsules: Metal–organic frameworks locked by size-matching ligand bolts. *Angew. Chem. Int. Ed.* **54**, 5966–5970 (2015).

44. B. Gui, X. Meng, Y. Chen, J. Tian, G. Liu, C. Shen, M. Zeller, D. Yuan, C. Wang, Reversible tuning hydroquinone/quinone reaction in metal–organic framework: Immobilized molecular switches in solid state. *Chem. Mater.* **27**, 6426–6431 (2015).

45. A. Modrow, D. Zargarani, R. Herges, N. Stock, The first porous MOF with photoswitchable linker molecules. *Dalton Trans.* **40**, 4217–4222 (2011).

46. J. Park, D. Yuan, K. T. Pham, J.-R. Li, A. Yakovenko, H.-C. Zhou, Reversible alteration of CO_2 adsorption upon photochemical or thermal treatment in a metal–organic framework. *J. Am. Chem. Soc.* **134**, 99–102 (2012).

47. J. W. Brown, B. L. Henderson, M. D. Kiesz, A. C. Whalley, W. Morris, S. Grunder, H. Deng, H. Furukawa, J. I. Zink, J. F. Stoddart, Photophysical pore control in an azobenzene-containing metal–organic framework. *Chem. Sci.* **4**, 2858–2864 (2013).

48. Z. Wang, L. Heinke, J. Jelic, M. Cakici, M. Dommaschk, R. J. Maurer, H. Oberhofer, S. Grosjean, R. Herges, S. Bräse, K. Reuter, C. Wöll, Photoswitching in nanoporous, crystalline solids: An experimental and theoretical study for azobenzene linkers incorporated in MOFs. *Phys. Chem. Chem. Phys.* **17**, 14582–14587 (2015).

49. J. H. Cavka, S. Jakobsen, U. Olsbye, N. Guillou, C. Lamberti, S. Bordiga, K. P. Lillerud, A new zirconium inorganic building brick forming metal organic frameworks with exceptional stability. *J. Am. Chem. Soc.* **130**, 13850–13851 (2008).

50. D. Cunha, M. Ben Yahia, S. Hall, S. R. Miller, H. Chevreau, E. Elkaïm, G. Maurin, P. Horcajada, C. Serre, Rationale of drug encapsulation and release from biocompatible porous metal–organic frameworks. *Chem. Mater.* **25**, 2767–2776 (2013).

51. Y. Chen, Y. Liu, Cyclodextrin-based bioactive supramolecular assemblies. *Chem. Soc. Rev.* **39**, 495–505 (2010).

52. M. V. Rekharsky, Y. Inoue, Complexation thermodynamics of cyclodextrins. *Chem. Rev.* **98**, 1875–1918 (1998).

53. A. Schaate, P. Roy, A. Godt, J. Lippke, F. Waltz, M. Wiebcke, P. Behrens, Modulated synthesis of Zr-based metal–organic frameworks: From nano to single crystals. *Chemistry* **17**, 6643–6651 (2011).

54. X. Y. Hu, K. Jia, Y. Cao, Y. Li, S. Qin, F. Zhou, C. Lin, D. Zhang, L. Wang, Dual photo- and pH-responsive supramolecular nanocarriers based on water-soluble pillar[6]arene and different azobenzene derivatives for intracellular anticancer drug delivery. *Chemistry* **21**, 1208–1220 (2015).

Science Advances

Mechanized azobenzene-functionalized zirconium metal-organic framework for on-command cargo release

Xiangshi Meng, Bo Gui, Daqiang Yuan, Matthias Zeller and Cheng Wang

ARTICLE TOOLS	http://advances.sciencemag.org/content/2/8/e1600480
SUPPLEMENTARY MATERIALS	http://advances.sciencemag.org/content/suppl/2016/08/01/2.8.e1600480.DC1
REFERENCES	This article cites 54 articles, 4 of which you can access for free http://advances.sciencemag.org/content/2/8/e1600480#BIBL
PERMISSIONS	http://www.sciencemag.org/help/reprints-and-permissions

Use of this article is subject to the Terms of Service